Supplement of Atmos. Chem. Phys., 26, 3881–3900, 2026
https://doi.org/10.5194/acp-26-3881-2026-supplement

Atmospheric Chemistry and Physics
Open Access
EGU

Supplement of

Assessment and prediction of dust emissions, deposition and radiation forcing in Central Asia

Ying Gan et al.

Correspondence to: Zhe Zhang (zhangzhe_0110@yeah.net)

S1. SBDART with solar photometer verification

Our study, conducted with thoroughness and precision, aims to more accurately evaluate the quality of the direct radiative forcing (ADRF) data calculated by the SBDART radiation transfer model in Central Asia. We comprehensively compare and analyze the radiation flux data at each site simulated by the SBDART model with the upward and downward radiation fluxes in the radiative forcing provided by the solar photometer observation network.

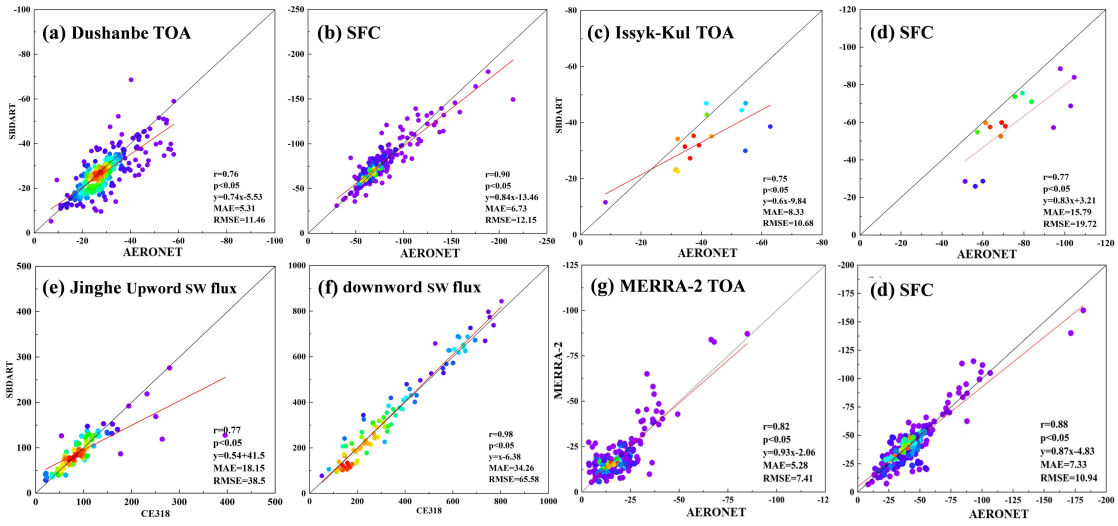

Fig. S1. Linear fits of short-wave radiation fluxes obtained by SBDART, MERRA-2 and the solar photometer.

S2.Historical spatial distribution of dust emissions and deposition under different CMIP6 scenarios

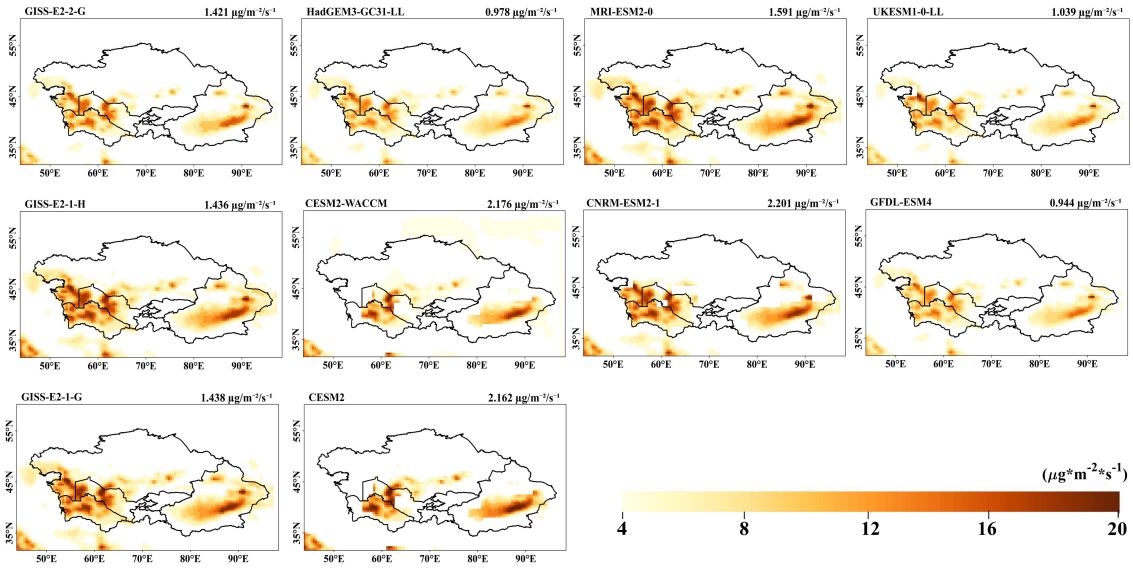

Fig. S2. Historical spatial distribution of dust emissions and deposition from CMIP6 models.

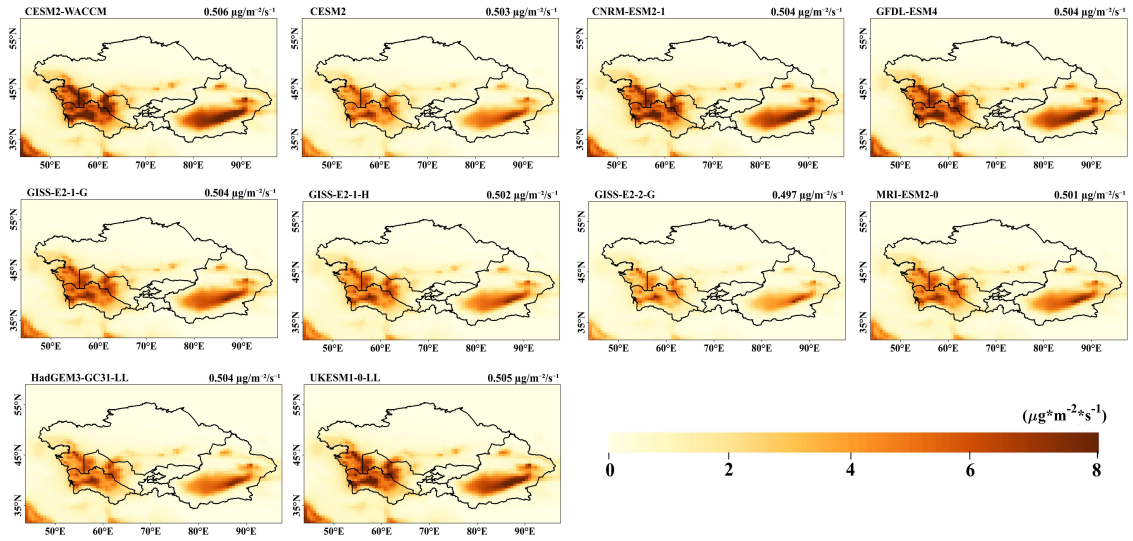

Fig. S3. Historical spatial distribution of dry deposition of dust in Central Asia in 10 CMIP6 models.

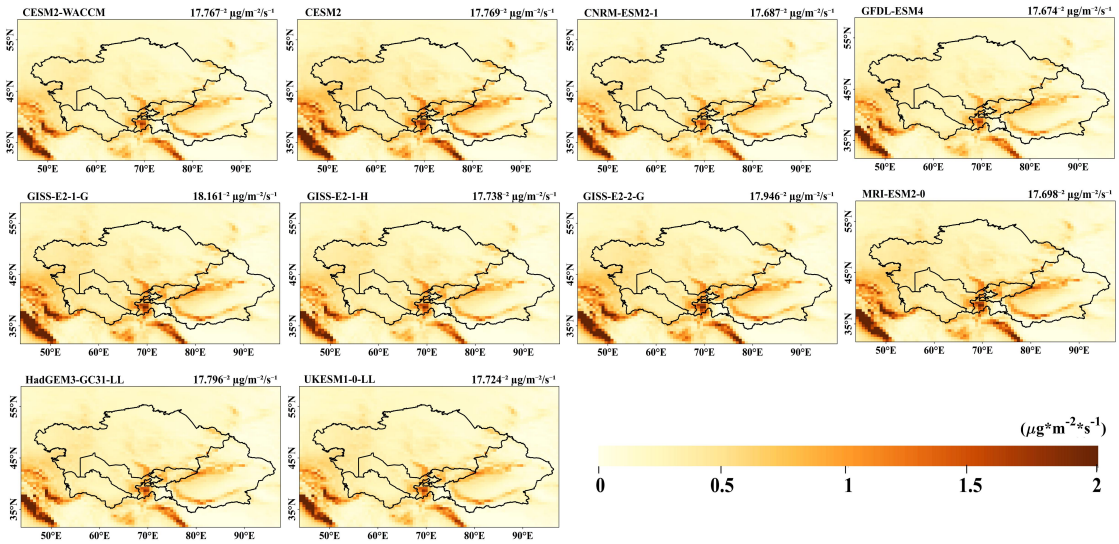

Fig. S4. Historical spatial distribution of wet deposition of dust in Central Asia under 10 CMIP6 models

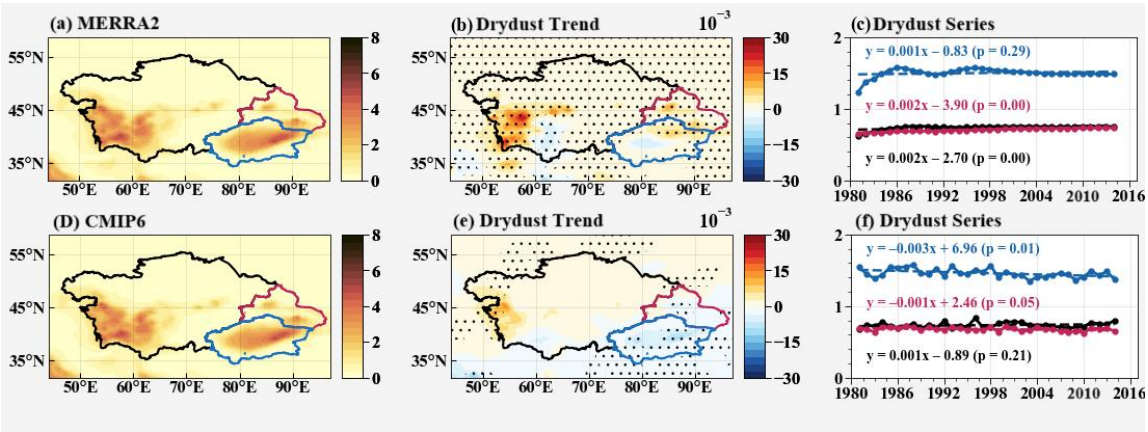

Fig. S5. Spatial distribution, linear trends, and time series of dust dry deposition from MERRA-2 and the CMIP6 multi-model ensemble (MME) over Central Asia during 1980–2014. Red outlines Northern Xinjiang, blue outlines Southern Xinjiang, and black outlines the five Central Asian countries in panels (b) and (e). Black dots indicate regions significant at the 95% confidence level.

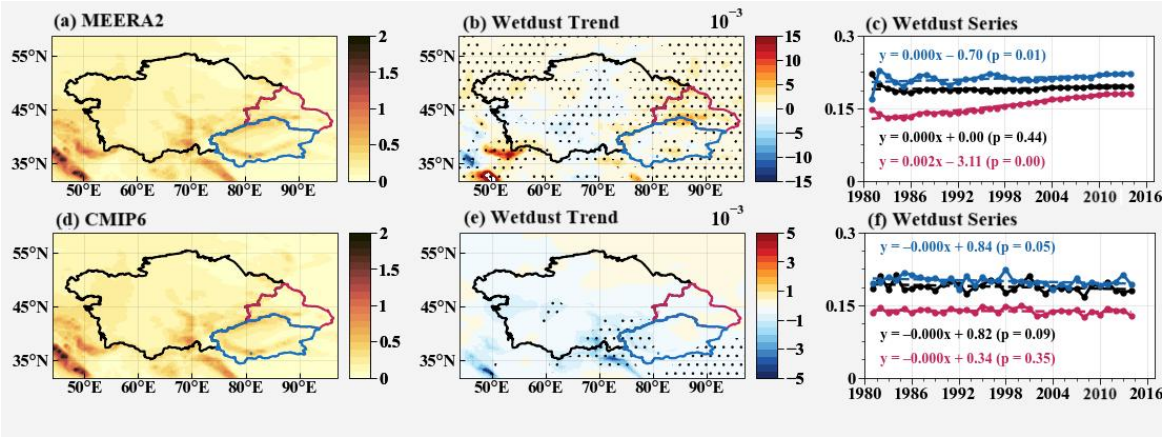

Fig. S6. Spatial distribution, linear trends, and time series of dust wet deposition from MERRA-2 and the CMIP6 multi-model ensemble (MME) over Central Asia during 1980–2014. Red outlines Northern Xinjiang, blue outlines Southern Xinjiang, and black outlines the five Central Asian countries in panels (b) and (e). Black dots indicate regions significant at the 95% confidence level.

S3. Future projections of wet and dry deposition based on the CMIP6 multimodel ensemble mean

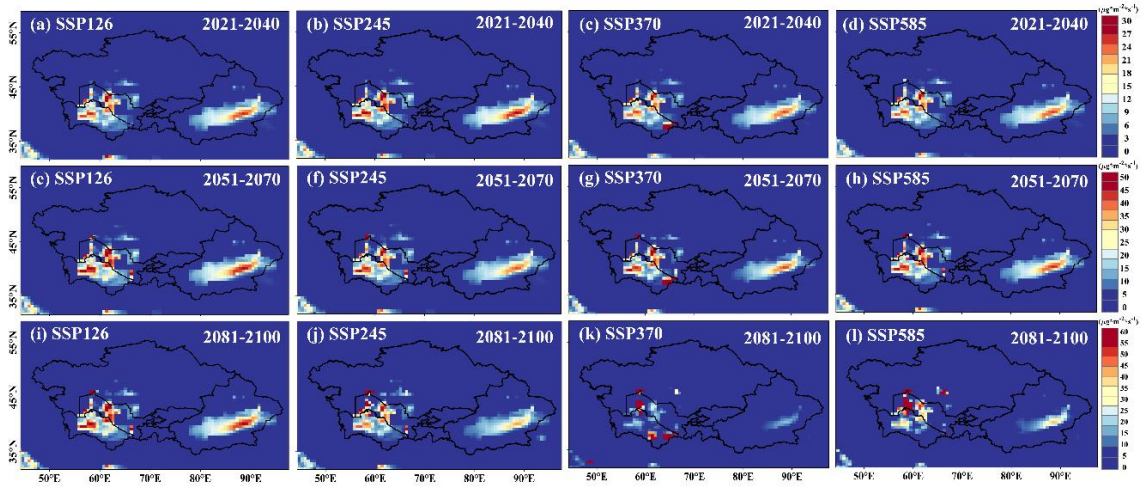

Fig. S7. Future changes in dust emissions during different periods. Spatial variations in the absolute values of dust emissions over Central Asia under four CMIP6 MME SSP scenarios: (a–d) near future (2021–2040), (e–h) medium term (2051–2070), and (i–l) long term (2081–2100), relative to the historical baseline (2000–2014).

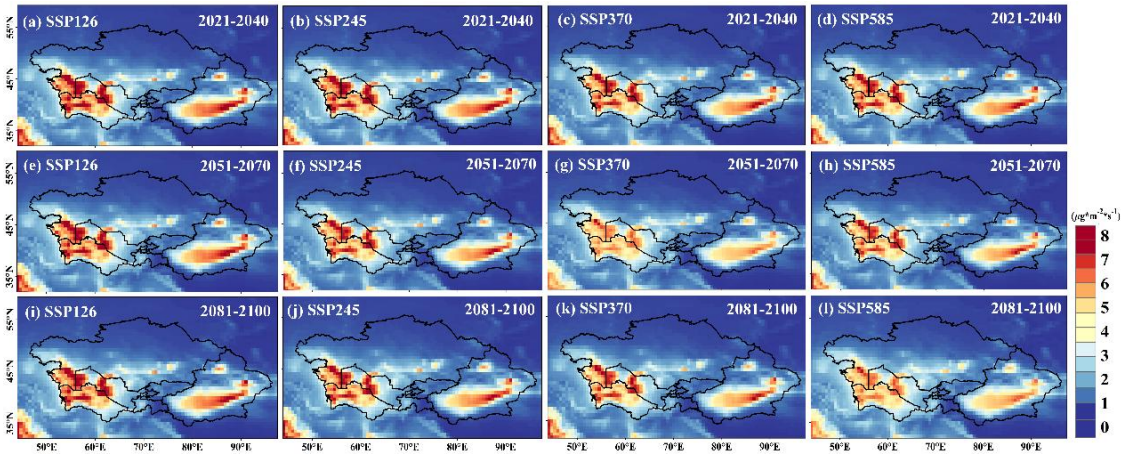

Fig. S8. Future changes in total dust deposition during different periods. Spatial variations in the absolute values of total dust deposition over Central Asia under four CMIP6 MME SSP scenarios: (a–d) near future (2021–2040), (e–h) mid-century (2051–2070), and (i–l) long term (2081–2100), relative to the historical baseline (2000–2014).

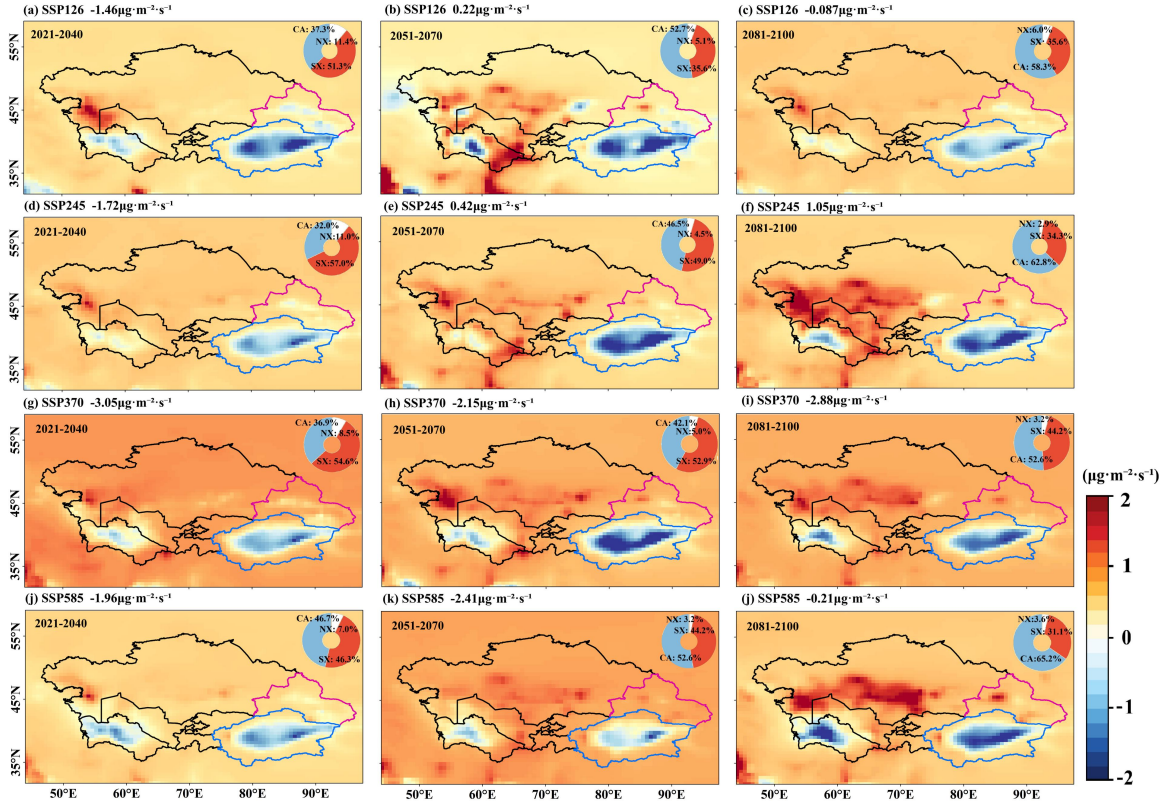

Fig. S9. Future changes in dry deposition of dust at different times. Spatial variations of dust-dry deposition in Central Asia under the four CMIP6 MME SSP scenarios for (a–d) the recent period (2021–2040), (e–h) the medium term (2051–2070), and (i–l) the long term (2081–2100) relative to the historical period (2000–2014).

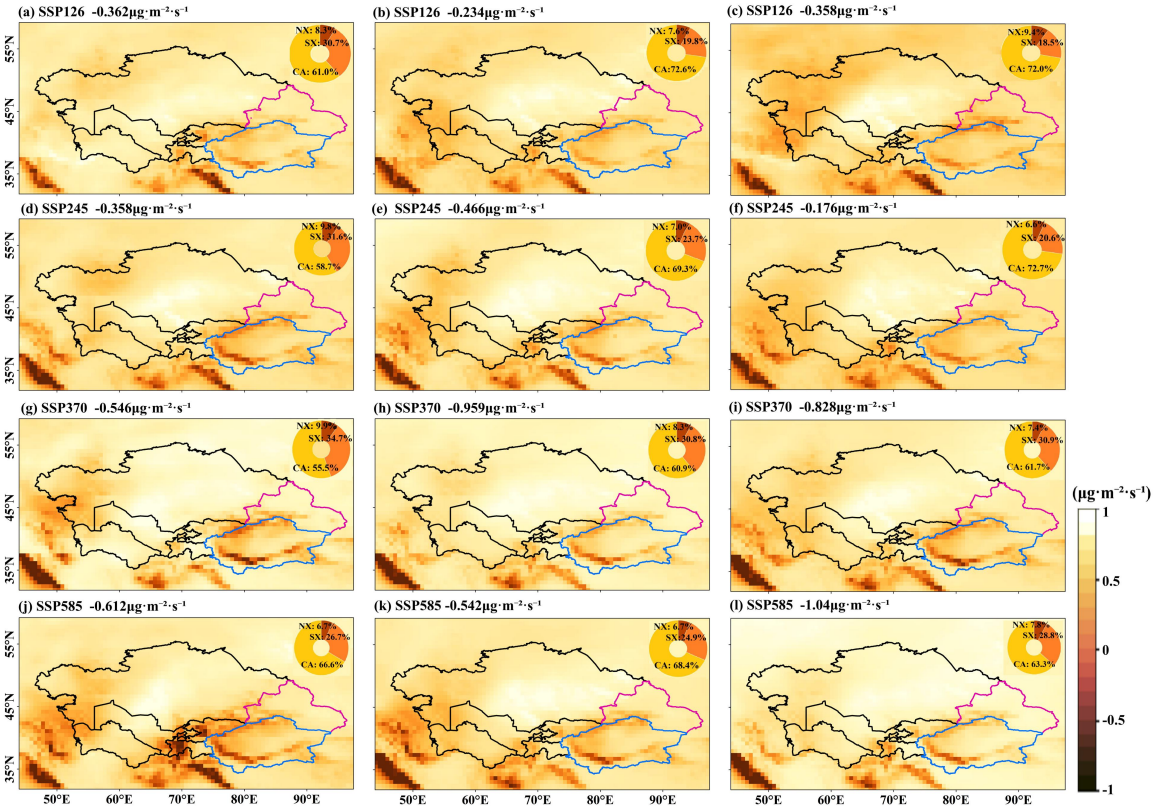

Fig. S10. Future changes in wet deposition of dust at different times. Spatial variations of wet dust deposition in Central Asia under the four CMIP6 MME SSP scenarios for (a–d) the recent period (2021–2040), (e–h) the medium term (2051–2070), and (i–l) the long term (2081–2100) relative to the historical period (2000–2014).

S4. SARIMA model prediction of direct radiative forcing of dust aerosols

To improve conciseness, five representative diagnostic maps from Southern Xinjiang are presented here as examples. The results of the maps in other regions are similar. For specific data, please refer to the appendix.

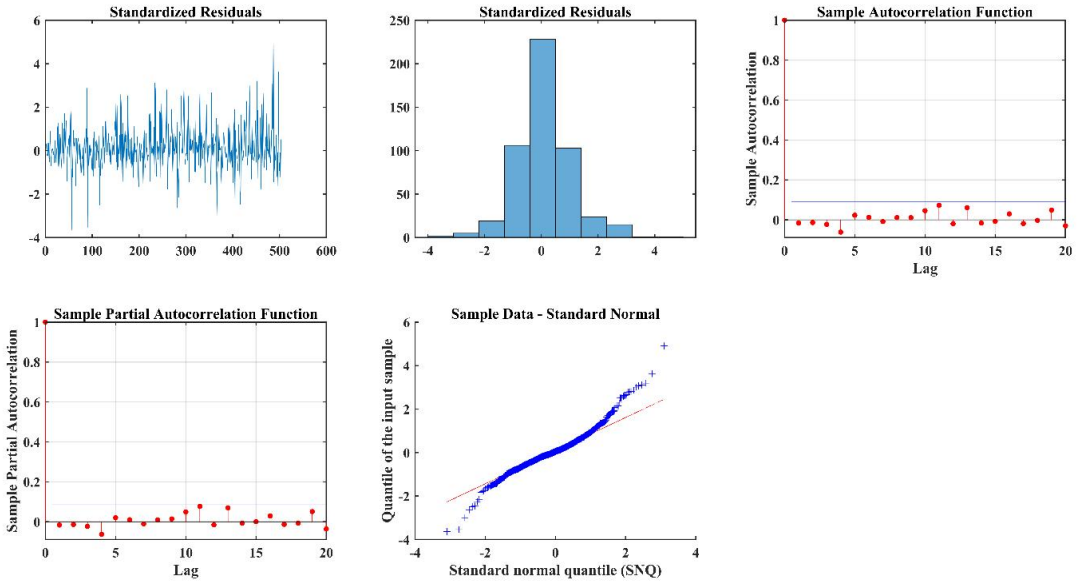

Fig. S11. Diagnostic results of SARIMA sample.

S5. Uncertainty analysis between different CMIP6 models and MERRA-2 data.

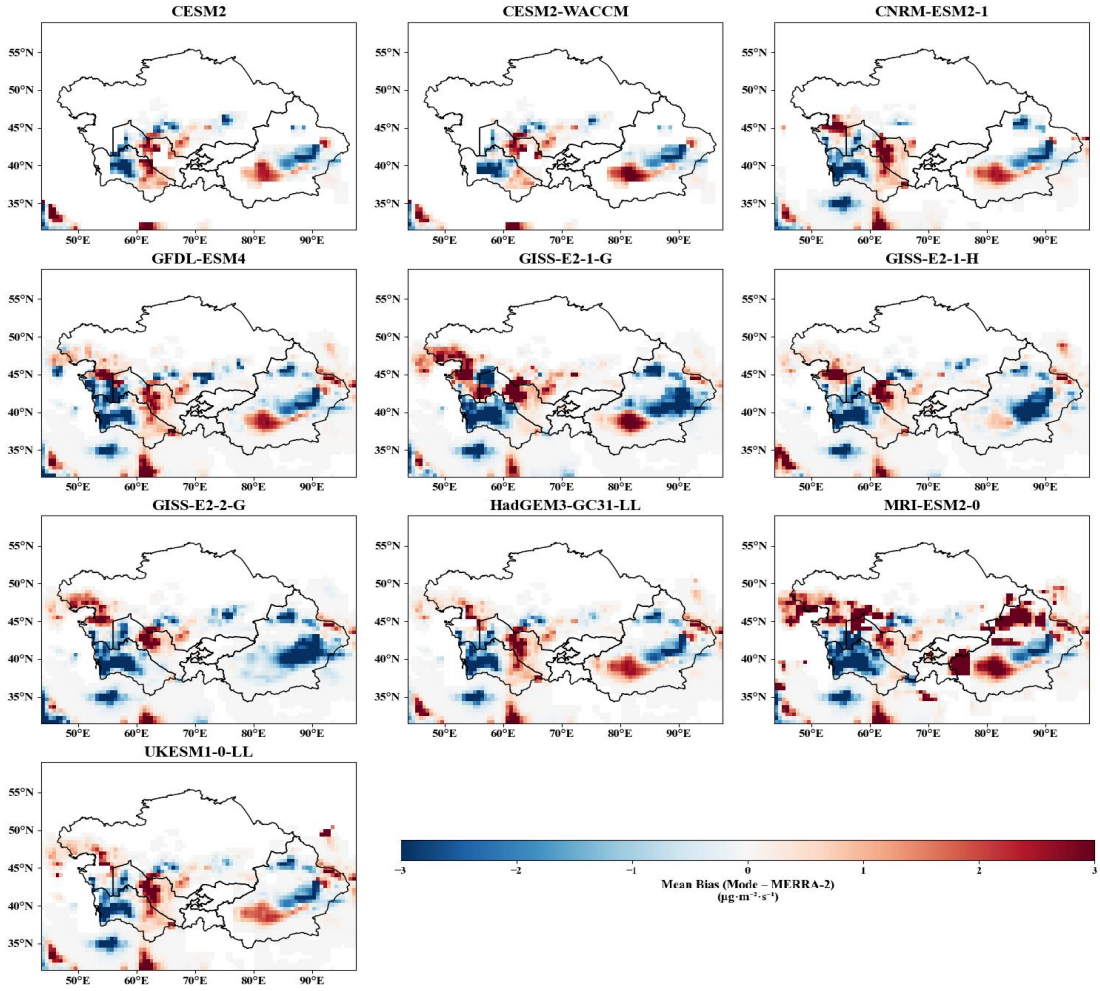

Fig. S12. Spatial distribution of deviations between 10 CMIP6 models and MERRA-2 data.

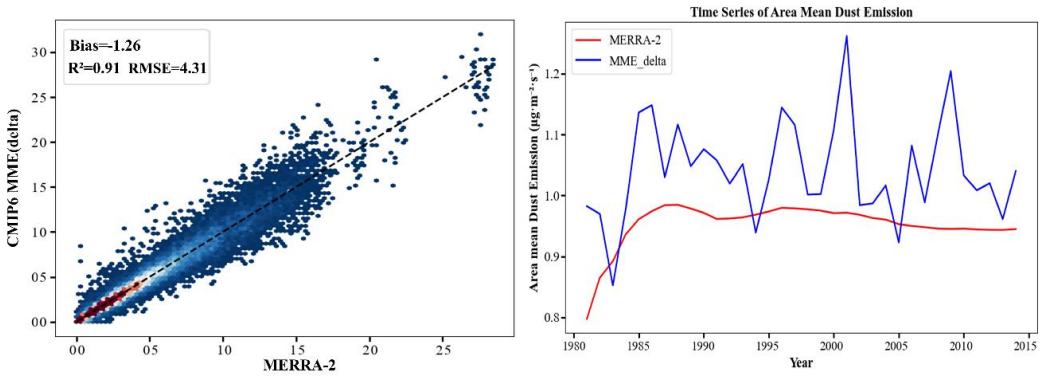

Fig. S13. Pixel-wise linear regression results between the CMIP6 multi-model ensemble (MME) and MERRA-2 data (a), along with the corresponding time series.